



Gas hydrate powder formation – Ultimate solution in natural gas flow assurance



Minwei Sun^a, Abbas Firoozabadi^{a,b,*}

^a Reservoir Engineering Research Institute, 595 Lytton Avenue, Suite B, Palo Alto, CA 94301, USA

^b Yale University, 9 Hillhouse Avenue, New Haven, CT 06511, USA

HIGHLIGHTS

- We demonstrate gas hydrate powder formation for the first time.
- Hydrate volume fraction can be as high as 95% with fluidity features.
- The new anti-agglomerant shows kinetic inhibition effect.
- We propose a mechanism for the formation of hydrate powders.

ARTICLE INFO

Article history:

Received 7 October 2014

Received in revised form 20 December 2014

Accepted 22 December 2014

Available online 10 January 2015

Keywords:

Flow assurance

Gas hydrates

Anti-agglomeration

Hydrate powder

Energy storage

ABSTRACT

Gas hydrates may plug hydrocarbon flowlines even at low hydrate volume fraction due to agglomeration. Anti-agglomeration is perhaps the most effective approach for flow assurance. An effective anti-agglomerant (AA) can prevent gas hydrate particles from sticking together by lowering of the water–oil interfacial tension and increase of the contact angle of water on hydrate surface. In a recent work, we have introduced a new AA formulation which is effective; it forms hydrate slurry over a broad range of oil to water ratio. In this study, we introduce a modified chemical formulation effective at extreme conditions when hydrate powders are formed from two different gases. The formation of hydrate powders has not been reported in the literature. The powders flow readily in rocking cells. The hydrate fraction can be as high as 95% with fluidity behavior. The AA effectiveness reported in this study is much higher than the past work. A new anti-agglomeration mechanism is also proposed. The gas hydrate powder formation may have applications not only in flow assurance, but also in energy storage.

© 2014 Elsevier Ltd. All rights reserved.

1. Introduction

Gas hydrates are ice-like crystalline solids, in which small gas molecules are trapped inside the cages formed by water molecules [1]. The hydrate surface is inherently hydrophilic [2]. A thin layer of liquid water film is present on the hydrate surface [3], which leads to a capillary bridge between hydrate particles [2,4]. The strong capillary force holds the particles together, causing agglomeration and high risks of pipeline blockage in hydrocarbon production. Gas hydrate formation has been a major challenge in flow

assurance, especially at high pressure and low temperature typically in seabed conditions [5].

The capillary force (F_C) in the liquid bridge between two hydrate particles depends on water–oil interfacial tension (σ) and contact angle (θ_p) of the capillary liquid on the hydrate surface as described by [5]

$$\frac{F_C}{r} = 2\pi\sigma \cos \theta_p$$

where r is the hydrate particle radius, assuming hydrate particles are spheres. Anti-agglomerants (AAs) reduce the capillary force by lowering the water–oil interfacial tension and increasing contact angle [6–9]. When the capillary force is weaker than the shearing force in the flow, hydrate particles are carried by the liquid as a slurry. In a recent work [10], we have compared few AAs that all reduce the water–oil interfacial tension significantly. However, the performances are very different. The contact angle of water on

Abbreviations: AA, anti-agglomerant.

* Corresponding author at: Yale University, 9 Hillhouse Avenue, New Haven, CT 06511, USA. Tel.: +1 203 432 4379; fax: +1 203 432 4387.

E-mail addresses: msun@rerinst.org (M. Sun), abbas.firoozabadi@yale.edu (A. Firoozabadi).

hydrate surface is close to 0 [6]. Adsorption of AA molecules increases contact angle and alters the surface to less water-wetting. The chemical structure and functional groups of AAs determine the binding force onto hydrate particles, which affect the contact angle and AA performance. An effective AA keeps hydrates as slurry in water or in hydrocarbon phase. The hydrate slurry turns into a paste as the hydrate volume fraction increases, as observed in our recent study [10] and the work of others [2,11]. Blockage occurs when the hydrate particles are closely packed, reaching maximum packing fraction. The close-packing of equal-size spheres has a volume fraction of 0.74. The maximum packing fraction in hydrate systems is believed to be 0.6–0.7 [2]. However, plugging could occur at lower hydrate volume fraction in reality [11,12]. When gas hydrates form in a pipeline, the crystalline particles stick together and turn into large aggregates with a fractal structure. They trap the aqueous phase and liquid hydrocarbon phases in the internal pores [1,2]. Effective AAs prevent agglomeration, thus allowing formation of a hydrate slurry. When the hydrate volume fraction is high (e.g., >0.50), no slurry can be formed at the usual hydrophilic conditions. When all the water is converted into hydrates and the liquid condensate or the oil phase is small, no solution to hydrate flow assurance by anti-agglomeration has been discussed in the literature.

Matsumoto et al. have reported slush ice with ice packing factor (IPF) higher than 70% by using silane-couplers and silicone oil [13]. They have added 4% silane-coupler into a mixture of 90% water and 10% silicone oil (volume basis) and cooled the mixture while stirring at 200 rpm. The ice surface is covered by silane-couplers and oil. Capillary bridge formation among ice particles is probably prevented. To the best of our knowledge, no hydrate powder formation in flow assurance has been reported. Hydrate powder formation is perhaps the only solution with AA at the conditions that all the water is converted to hydrates and the amount of the condensate liquid or the oil phase is small.

There are three types of instruments for hydrate formation and inhibition tests: rocking cells, autoclaves and flow loops [14]. Flow loops are closest to field conditions. However, they require large amount of fluids and gases; the requirement limits their applications. Autoclaves are temperature-controlled steel cell with stirring. They usually require several hundred milliliters of fluids for each test. High pressure rocking cells use small sapphire cells as reactors, which normally require no more than 50 milliliters per test. A stainless steel ball in the cylindrical cell provides agitation during rocking. Clear sapphire tubes allow direct visual observations during tests. Rocking cells are considered a conservative test because of the low shearing force during rocking compared to the other two methods. We employ rocking cells due to simplicity and the ability for visual observation.

In this work, we report the formation of hydrate powders from two different gases and our new AA formulation at a hydrate volume fraction as high as 0.95. We also suggest a new mechanism for the hydrate powder formation.

2. Material and methods

A rocking cell instrument is used for gas hydrate tests as described in our recent work [10,15]. A schematic diagram and image of the setup is shown in Fig. S1 of the Supplementary Information. The cells are closed during rocking. In all tests, water content is low, 2 or 3 mL H₂O along with 0.02–2 mL *n*-octane. The fluids are loaded in the 20-mL sapphire cells. All the water converts to gas hydrates in the cell. Two different gases are used as hydrate formers: a mixture of methane and propane (Gas 1), and a natural gas (Gas 2) containing 81.0% methane, 8.3% ethane, 4.8% propane, 2.4% CO₂ and 3.5% other species (by mol). For Gas 1, the cell is charged with propane first to the initial watercut before being

charged with methane to a desired initial pressure. The rocking frequency is set to 15 times/min. The bath temperature, pressure and ball running time during rocking are recorded. At the start after charging the cells with test mixtures, they are rocked at 20 °C (24, or 28 °C) for half an hour to reach equilibrium. This is set as the initial condition of the closed cell test. Then the water bath is cooled from room temperature to 2 °C for Gas 1 (4 °C for Gas 2) at rate of either –2 °C/h or –10 °C/h, while the cells are being rocked. They are then kept at 2 °C for Gas 1 (4 °C for Gas 2) for a period of time allowing the gas hydrates to fully develop before the temperature ramps back to the initial temperature. Sharp pressure changes indicate hydrate formation/dissociation. A long ball running time implies high viscosity in the cell. The steel ball stops running when hydrate plugging occurs. The effectiveness is evaluated by visual observations and by ball running time. It should be noted that all the water turns into gas hydrates in our tests at the low testing temperature.

The hydrate tests for Gas 1 are listed in Table 1. Under test conditions, the slurry hydrate forms. Our AA (from Lubrizol Corporation) contains 80–89% cocamidopropyl dimethylamine (as the effective component), 5–10% glycerin, small amount of free amine and water. AA dosage is 0.5 wt% in water in all tests. The initial pressure varies from 40 to 100 bar. After charging the cells with gas, the initial watercut is estimated to be in the range of 25–66% by considering the formation of liquid condensate. The hydrate volume fraction at 2 °C is higher because some of the condensate species become part of the hydrates; the hydrate density is less than water density.

3. Results and discussion

3.1. Gas hydrates from Gas 1

In all the tests, our AA shows both anti-agglomeration and kinetic inhibiting effects during hydrate formation. The mixture in the cells flows in the form of hydrate slurry, or hydrate powders when the hydrate volume fraction is high. The hydrate dissociation temperatures are above 15 °C, indicating a large subcooling since the testing temperature is low at 2 °C. The low hydrate formation temperatures at high pressure in all the tests demonstrate the kinetic effect. Let us describe Test 12 in Table 1 in which the initial mixture consists of 2 mL of water at 0.5 wt% concentration of AA, 0.02 mL *n*-octane and 1 mL propane liquid. This gives approximate initial watercut (water volume% in total liquid) of 66%. The initial pressure is 100 bar at 28 °C. Hydrate starts to form at 18.8 °C and 93.7 bar indicated by the sudden pressure drop during cooling, shown in Fig. 1. The pressure drops to 78 bar at 2 °C, 17 °C below the hydrate formation temperature. There is no decrease of pressure at 2 °C which indicates no further hydrate formation. All the water is converted into hydrates at this condition. The ball running time is low throughout the test (red¹ curve in Fig. 1).

Hydrate powders are observed instead of hydrate slurry in Test 12. Fig. 2 shows that the hydrate powders move along with the stainless steel ball (in blue circle) during rocking. Four pictures are taken in 1 s. There is no free water left in the cell. The hydrate powders are loosely packed. They flow in the cell as shearing force is applied. Hydrate content in the mixture is estimated to be higher than 66%. To the best of our knowledge, this is the first report of anti-agglomeration of hydrates in the form of powders. A microscope picture (Fig. 3) shows most of the hydrate particles are smaller than 5 μm. Upon heating, the hydrates start to dissociate at 23.8 °C and 92.0 bar during warming, which is 5 °C higher than

¹ For interpretation of color in Fig. 1, the reader is referred to the web version of this article.

Table 1
Tests of low water content at AA concentration of 0.5 wt% in water (Gas 1: C1 + C3).

| Test # | Water (mL) | <i>n</i> -octane (mL) | Initial C3 condensate (mL) | Initial pressure (bar) | Initial temperature (°C) | Initial watercut | Hydrate formation (°C, bar) | Hydrate dissociation (°C, bar) | Cooling rate (°C/h) |
|--------|------------|-----------------------|----------------------------|------------------------|--------------------------|------------------|-----------------------------|--------------------------------|---------------------|
| 1 | 2 | 2 | 1 | 40 | 20 | 40% | 10.2, 36.8 | 17.3, 29.2 | -2 |
| 2 | 2 | 2 | 2 | 60 | 24 | 33% | 14.8, 57.2 | 20.6, 51.0 | -2 |
| 3 | 2 | 2 | 3 | 80 | 24 | 29% | 17.4, 76.9 | 22.3, 71.4 | -2 |
| 4 | 2 | 2 | 4 | 100 | 28 | 25% | 17.9, 92.5 | 23.6, 88.3 | -2 |
| 5 | 3 | 1 | 1 | 40 | 20 | 60% | 12.0, 37.5 | 15.8, 23.8 | -2 |
| 6 | 3 | 1 | 2 | 60 | 24 | 50% | 15.7, 57.2 | 19.8, 44.4 | -2 |
| 7 | 3 | 1 | 3 | 80 | 24 | 43% | 16.7, 75.8 | 21.8, 62.0 | -2 |
| 8 | 3 | 1 | 4 | 100 | 28 | 38% | 17.6, 92.3 | 23.0, 83.5 | -2 |
| 9 | 2 | 0.2 | 4 | 94 | 28 | 32% | 17.5, 88.5 | 23.1, 83.8 | -2 |
| 10 | 2 | 0.2 | 4 | 94 | 28 | 32% | 16.6, 87.0 | 23.4, 85.0 | -10 |
| 11 | 2 | 0.02 | 1 | 100 | 28 | 66% | 19.2, 93.9 | 23.9, 91.0 | -2 |
| 12 | 2 | 0.02 | 1 | 100 | 28 | 66% | 18.8, 93.7 | 23.8, 92.0 | -10 |

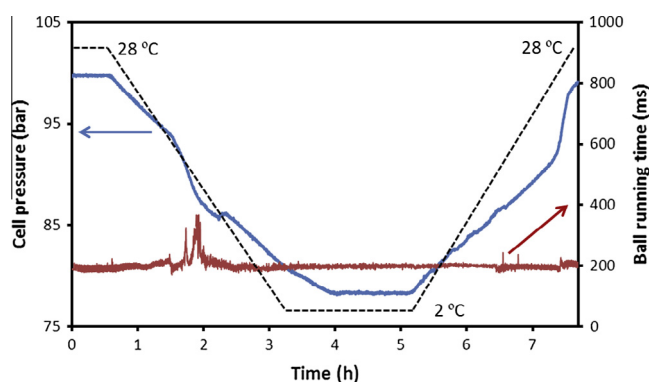


Fig. 1. Hydrate Test 12 (Gas 1). Hydrate formation from the initial pressure of 100 bar and the initial temperature of 28 °C. The temperature decreases from 28 °C to 2 °C at the rate of -10 °C/h, then kept at 2 °C for 2 h before ramping back to 28 °C. The cell contains 2 mL H₂O, 0.02 mL *n*-octane, 1 mL condensate liquid. The concentration of AA is 0.5 wt%.

hydrate formation temperature of 18.8 °C at 93.7 bar. There is an appreciable kinetic inhibiting effect. The induction time for hydrate formation in most of our tests varies from 0.5 to 3.5 h depending on the test mixture compositions, initial pressure and cooling rate. The induction time can be roughly estimated from Tables 1 and 2 by the cooling rate and temperature difference between hydrate formation and dissociation temperature. Generally, hydrate dissociation conditions are close to equilibrium. Comparison of the hydrate formation conditions to dissociation provides an estimate of the kinetic effect. The hydrate dissociation occurs at a lower pressure than hydrate formation. As a result, the equilibrium hydrate formation temperature should be higher than the dissociation temperature.

3.2. Gas hydrates from Gas 2

The natural gas used in this work introduces complications because of the acid gases, e.g., CO₂. In this work, we use a natural



Fig. 2. Hydrate Test 12 (Gas 1). Images of hydrate powders movement along the steel ball during rocking test. Images are taken at 8.5 °C and 88 bar. The process happens in less than 1 s. The blue circle shows the positions of steel ball. (For interpretation of the references to colour in this figure legend, the reader is referred to the web version of this article.)

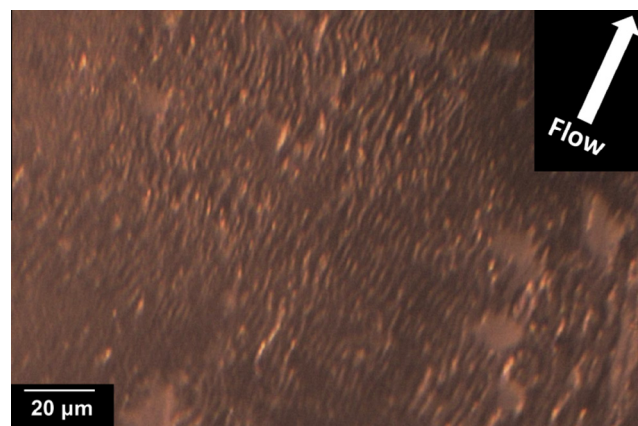
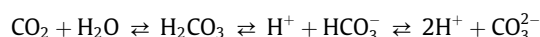
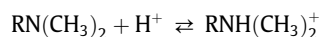


Fig. 3. Hydrate Test 12 (Gas 1). Microscope image of hydrate powders described in Fig. 2.

gas containing 2.4% CO₂ which lowers the pH of the aqueous solution as a result of the following reactions



Our surfactant molecule, a nonionic amine, reacts with H⁺ as follows,



The above reaction affects the AA performance. There is an increase in solubility of the surfactant in water at low pH. To investigate further we prepare an aqueous solution of 0.5% AA and 0.2% HCl, which has a pH value of 1.7. The reaction between HCl and the AA increases the interfacial tension between *n*-octane and aqueous phase from 5.6 mN/m to 10.9 mN/m. The high interfacial tension increases the capillary force which holds hydrate particles together. In our surfactant, the nitrogen atom provides the bonding site onto hydrate surface by forming N···H hydrogen bonds. At lower pH, the H⁺ weakens hydrogen bonds, thus reducing adsorp-

Table 2

Tests of low water content with AA concentration of 0.5 wt% in water and 4.0 wt% NaOH (Gas 2: natural gas).

| Test | Water (mL) | <i>n</i> -octane (mL) | Initial pressure (bar) | Initial Temp. (°C) | Initial watercut (%) | Hydrate formation (°C, bar) | Hydrate dissociation (°C, bar) | Cooling rate (°C/h) |
|------|------------|-----------------------|------------------------|--------------------|----------------------|-----------------------------|--------------------------------|---------------------|
| 1 | 2 | 0.1 | 67.5 | 20 | 95 | 7.6, 62.7 | 12.6, 57.3 | −4 |
| 2 | 2 | 0.1 | 67.5 | 20 | 95 | 7.4, 62.6 | 12.7, 57.3 | −10 |
| 3 | 2 | 0 | 68.4 | 20 | 100 | 9.0, 64.8 | 11.9, 54.9 | −4 |
| 4 | 2 | 0 | 68.4 | 20 | 100 | 8.8, 64.5 | 11.8, 54.8 | −10 |

tion onto hydrate surface. Consequently, the AA becomes less effective at low pH. A systemic study shows that a pH above 9 is required for our AA to be effective [15]. We introduce a small amount of NaOH into our formulation to neutralize the acidity. Because of high gas/water ratio in our tests and the high concentration of CO₂ (2.4%), 4.0 wt% NaOH is used in the following tests. The pH values after the tests are in the range of 9.6–9.8. We have found another base to replace NaOH in the AA formulation. With the new base the concentration is lowered significantly. The work will be published in the future.

Table 2 presents four sets of tests at high water to total liquid volumes (>95%). The testing cells are cooled from room temperature to 4 °C. Hydrate powders are observed in all the tests when the cells are kept at 4 °C for 24 h. The kinetic effect is more pronounced in the tests with 5 volume% *n*-octane. The hydrate crystallization temperature is 1.5 °C lower than the tests without *n*-octane. As discussed above, rapid adsorption of AA molecules onto hydrate surface is facilitated through oil-in-water emulsions.

Fig. 4 presents the pressure and ball running time profiles of test 3 in Table 2. There is no pressure decrease in the final 2 h at 4 °C, implying all the water is converted into gas hydrates. During the test, the steel ball and hydrate powders move inside the cell. However, in the period of 5–6.4 h and 16.8–19.5 h, the ball is temporarily stuck by hydrate. Stronger shearing force in flowlines than in the rocking cells helps with hydrate powder flow.

3.3. Proposed mechanism

The mechanism of hydrate powder formation can be explained as follows. Once the hydrate particles form, the AA molecules are absorbed onto the particle surface by hydrogen bonding which create a hydrophobic layer. Due to the attractions with hydrophobic tails of the AA molecules, the hydrocarbons in the system then form a coating on the hydrate particles as depicted in Fig. 5. The presence of the surfactants and hydrocarbons on the hydrate surface reduces the capillary force among the hydrate particles. The

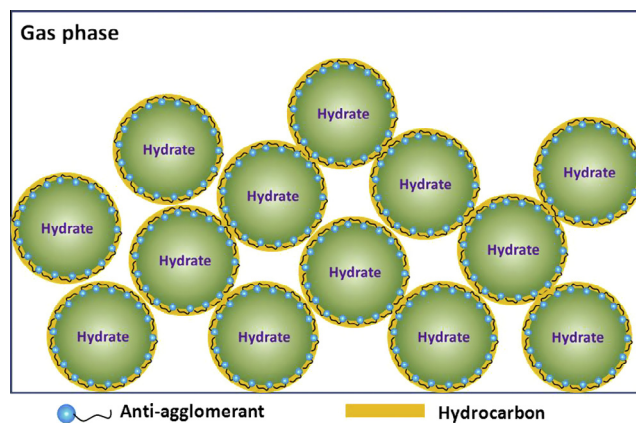


Fig. 5. Proposed mechanism of hydrate powder formation.

key to AA performance is their quick adsorption onto the hydrate particle surface and strong binding force between AA molecules and hydrates. We are currently performing molecular dynamics simulations to shed light into basic mechanisms.

There is a small amount of *n*-octane in our formulation in the test in Gas 1. Without *n*-octane, no “dry” hydrate powder is formed. Our AA has low solubility in water but molecularly dissolves in *n*-octane. The CMC of the AA surfactant in water is 30 ± 3 ppm. The size of micelles measured by dynamic light scattering is 8.8 ± 1.3 nm. However, when AA concentration is 0.5 wt% in water, most surfactant molecules form a rich phase as a thin top layer if the system is allowed to be still. After 2-min handshaking, the surfactant molecules form aggregates with the average size around 1 μm. Once 1.0 vol% *n*-octane is added, oil-in-water emulsions are formed with the size of 54.6 ± 4.9 nm. The emulsions facilitate even distribution of the surfactant molecules in the aqueous phase. This is the mechanism by which a small amount of *n*-octane enhances the effectiveness of our AA. In the tests with natural gas there is an appreciable amount of propane and heavier hydrocarbons. The heavier hydrocarbons play the same role as *n*-octane plays in Gas 1 in formation of a thin hydrocarbon liquid on the surface of hydrate particles when there are adsorbed surfactant molecules.

4. Conclusions

We report successful results in hydrate anti-agglomeration from a new AA formulation that leads to formation of hydrates powders at high water to liquid ratios (high watercuts) and high hydrate volume fractions. This is the first report of hydrate powder formation in the anti-agglomeration of natural gas hydrates with broad potential applications.

We also discover that a small amount of a liquid hydrocarbon (e.g., *n*-octane) can enhance the AA performance. The formation of oil-in-water emulsions makes AA molecules homogeneously distributed. Once hydrate particles form, those AA molecules bind onto the surface quickly. At high watercuts the powders can form

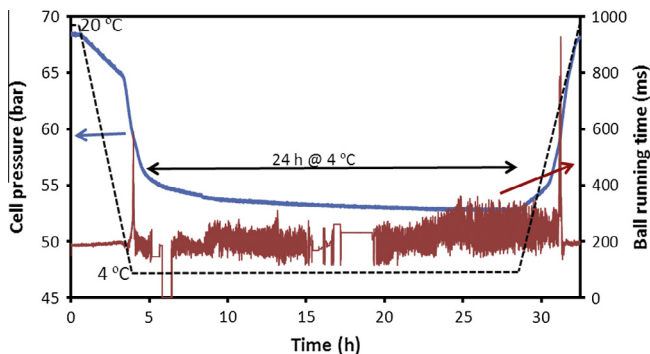


Fig. 4. Hydrate Test 3 (Gas 2). Hydrate formation from the initial pressure of 68.4 bar and the initial temperature of 20 °C. The temperature decreases from 20 °C to 4 °C at the rate of −4 °C/h, then kept at 4 °C for 24 h before ramping back to 20 °C. The cell contains 2 mL H₂O and 0.1 mL *n*-octane. The concentration of AA is 0.5 wt%. The concentration of NaOH is 4.0 wt%.

when there is a very small amount of hydrocarbon liquid (e.g., 1% by volume). We propose that a thin liquid hydrocarbon forms on the surface of the hydrate particle due to the presence of the AA tail.

Gas hydrate powder formation has not only applications in flow assurance of natural gases but may be also a promising candidate for energy storage.

Acknowledgment

We thank the member companies of the Reservoir Engineering Research Institute (RERI) for their financial support.

Appendix A. Supplementary material

A schematic diagram and image of rocking cells setup are presented in supplementary information. Supplementary data associated with this article can be found, in the online version, at <http://dx.doi.org/10.1016/j.fuel.2014.12.078>.

References

- [1] Sloan ED, Koh CA. *Clathrate Hydrates of Natural Gases*. CRC; 2008.
- [2] Colombel E, Gateau P, Barre L, Gruy F, Palermo T. *Oil Gas Sci Technol – Revue de l'IFP* 2009;64(5):629–36.
- [3] Jiménez-Ángeles F, Firoozabadi A. *J Phys Chem C* 2014;118(45):26041–8.
- [4] Austvik T, Li X, Gjertsen LH. *Ann NY Acad Sci* 2000;912(1):294–303.
- [5] Kelland MA. *Energy Fuels* 2006;20(3):825–47.
- [6] Anklam MR, York JD, Helmerich L, Firoozabadi A. *AIChE J* 2008;54(2):565–74.
- [7] Yang S-O, Kleehammer DM, Huo Z, Sloan ED, Miller KT. *J Colloid Interface Sci* 2004;277(2):335–41.
- [8] Taylor CJ, Dieker LE, Miller KT, Koh CA, Sloan Jr ED. *J Colloid Interface Sci* 2007;306(2):255–61.
- [9] Song JH, Couzis A, Lee JW. *Langmuir* 2010;26(12):9187–90.
- [10] Sun M, Firoozabadi A. *J Colloid Interface Sci* 2013;402:312–9.
- [11] Moradpour H, Chapoy A, Tohidi B. Transportability of hydrate particles at high water cut systems and optimisation of anti-agglomerant concentration. In: *Proceedings of the 7th International Conference on Gas Hydrates*; 2011.
- [12] Filippov AV, Zurita M, Rosner DE. *J Colloid Interface Sci* 2000;229(1):261–73.
- [13] Matsumoto K, Okada M, Kawagoe T, Kang C. *Int J Refrig* 2000;23(5):336–44.
- [14] Patel ZD, Russum J. *Offshore* 2010(6):70–2.
- [15] Sun M, Firoozabadi A. *Energy Fuels* 2014;28(3):1890–5.